Experiments to Determine the Wavelength of a HeNe Laser

Natalia Tabja[1]

[1] *Department of Physics, University of Toronto*

(Dated: March 17, 2025)

We measure the 633 nm HeNe laser wavelength using Fraunhofer diffraction through square and circular apertures, as well as reflection and transmission gratings. Aperture methods yield results within a few percent of 633 nm but suffer large uncertainties due to fringe selection and beam misalignment, while the reflection grating achieves closer agreement (1.3% error). These findings emphasize the importance of meticulous alignment and robust analysis in diffraction-based wavelength measurements.

Introduction

Huygens' Principle and Wave Propagation

Diffraction and interference phenomena can be understood using Huygens' principle, which states that every point on a wavefront acts as a secondary source of spherical wavelets. The new wavefront at a later time is the envelope of these secondary wavelets. Mathematically, the propagation of a field $E(x, y, z)$ from an aperture at $z = 0$ is described by the Fresnel-Kirchhoff diffraction formula:

$$E(x,y,z) = -\tfrac{i}{\lambda}\iint_{\text{aperture}} E(x',y',0)\tfrac{e^{ikR}}{R}\left[\tfrac{1+\cos(\mathbf{R},\hat{\mathbf{z}})}{2}\right]dx'dy'. \quad (1)$$

where $E(x', y', 0)$ is the field at the aperture, $k = \frac{2\pi}{\lambda}$ is the wave number, r is the distance between the aperture point (x', y') and observation point (x, y), and θ is the angle between the normal to the aperture and r. Since this integral is difficult to solve directly, approximations such as the Fresnel and Fraunhofer approximations are applied depending on the observation distance.

Fresnel and Fraunhofer Diffraction

Diffraction can be classified based on the distance z from the aperture to the observation plane.

The Fresnel approximation assumes that the denominator of the diffraction integral can be approximated as $R \approx z$ while keeping a quadratic term in the exponent. This is valid for relatively small angles and when the aperture is not too far from the observation plane.

Fraunhofer (far-field) diffraction occurs when

$$z \gg \frac{a^2}{\lambda}, \quad (2)$$

and the quadratic phase term $e^{i\frac{k}{2z}(x^2+y^2)}$ can be neglected. In this case, the diffraction integral reduces to a Fourier transform of the aperture field $E(x', y', 0)$ with respect to the spatial coordinates x' and y', mapping it into the spatial frequency domain defined by the wavevector components in the observation plane. In particular, we have

$$E(x,y,z) \propto \iint_{\text{aperture}} E(x',y',0)e^{-ik(xx'+yy')/z}dx'dy'. \quad (3)$$

where a is the characteristic size of the aperture. Under this assumption, we also invoke the small-angle approximation, meaning that $\sin\theta \approx \theta \approx \frac{x}{z}$ or $\frac{y}{z}$.

Rectangular Aperture Diffraction

For a rectangular aperture of width Δx and height Δy, the Fraunhofer diffraction pattern is given by:

$$I(x,y) = I_0\left(\operatorname{sinc}^2\left(\frac{\pi x\Delta x}{\lambda z}\right)\operatorname{sinc}^2\left(\frac{\pi y\Delta y}{\lambda z}\right)\right), \quad (4)$$

where

$$I_0 = \frac{nc\epsilon_0}{2}\left|E(x',y',0)\right|^2, \quad (5)$$

is the intensity at the aperture.

The position of the first minimum in the diffraction pattern, measured relative to the center of the zeroth-order fringe, is related to the wavelength by:

$$\lambda = \frac{\Delta x \cdot x}{z}, \quad \lambda = \frac{\Delta y \cdot y}{z}, \quad (6)$$

where x and y represent the distances to the first diffraction minimum in the horizontal and vertical directions, respectively.

Circular Aperture Diffraction (Airy Disk)

For a circular aperture of diameter D, the intensity distribution follows an Airy pattern:

$$I(\theta) = I_0\left(\frac{2J_1(kD\sin\theta)}{kD\sin\theta}\right)^2, \quad (7)$$

where J_1 is the first-order Bessel function. The first dark ring occurs at:

$$\theta_1 \approx 1.22\frac{\lambda}{D}. \tag{8}$$

For small angles, using $\sin\theta \approx \theta \approx \frac{\rho}{z}$, the corresponding fringe separation in the image plane is:

$$\rho = 1.22\frac{\lambda z}{D}. \tag{9}$$

Diffraction Gratings

A diffraction grating consists of a periodic array of slits or grooves that diffract incident light into roughly discrete directions, which we refer to as diffraction orders. The diffraction results a pattern of bright and dark fringes, as illustrated in Figure 1, which depicts this phenomenon for a transmission grating.

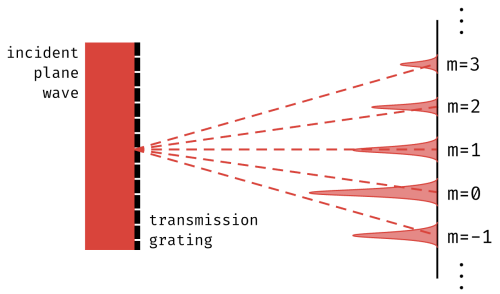

FIG. 1. Schematic of diffraction through a transmission grating, showing multiple diffraction orders.

The diffraction condition differs for transmission and reflection gratings. For a transmission grating, where light passes through slits and diffracts, the condition for constructive interference is given by:

$$m\lambda = d\sin(\theta_n), \tag{10}$$

where m is the diffraction order ($m = 0, \pm1, \pm2, \ldots$), d is the slit spacing (the inverse of the groove density), λ is the wavelength of incident light, and θ_n is the diffraction angle for the n^{th}-order fringe. In our setup, we measure the diffraction angle θ_1 by recording the fringe displacement Δy on a screen at a distance z from the grating:

$$\tan\theta_1 = \frac{\Delta y}{z}. \tag{11}$$

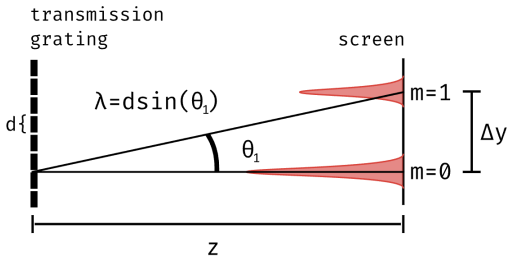

FIG. 2. Geometric representation of diffraction through a transmission grating, showing the first-order fringe separation.

For a reflection grating, where light is incident at an angle θ_i and diffracts upon reflection, the governing equation is:

$$m\lambda = d[\sin(\theta_i) + \sin(\theta_n)]. \tag{12}$$

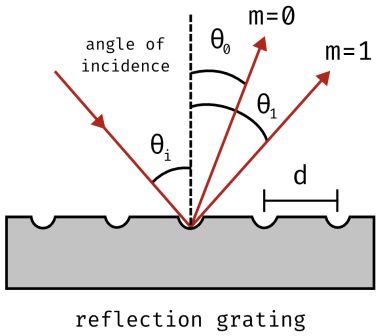

FIG. 3. Schematic of diffraction from a reflection grating, illustrating diffraction angles.

Here, θ_i is the angle of incidence and θ_n is the diffraction angle for the nth-order fringe. The summation accounts for both incident and diffracted wavefront angles relative to the grating. This equation applies regardless of whether the grating is blazed or not; however, a blazed grating is optimized to direct most of the diffracted light into a specific order. Once again, we choose to measure θ_1, since this is the easiest fringe to identify. Higher-order intensities are weaker, making measurements less reliable.

Experimental Goals

This experiment investigates diffraction patterns produced by laser light passing through square and circular apertures in the Fraunhofer regime, as well as diffraction from a reflection and transmission grating. The objectives are:

1. Determine the wavelength of the HeNe laser via analysis of imaged diffraction patterns (through

both a square and circular aperture) using the Fraunhofer approximation.

2. Determine the wavelength of the HeNe laser using diffraction from both a reflection and transmission grating, applying the diffraction grating equation to measure the angles of diffracted orders.

EXPERIMENTAL SETUP

Part 1: Diffraction Through an Aperture

The experimental setup is shown in Figure 4. A HeNe laser ($\lambda = 633$ nm, < 4 mW) [1] was used as the coherent light source. The laser beam was guided by mirrors toward an aperture mounted on a translation stage. The resulting diffraction pattern was recorded by a monochrome CMOS camera (Allied Vision Alvium 1800 U-500m) placed at a distance z from the aperture. The camera has a pixel size of $2.2 \times 2.2\,\mu$m[4].

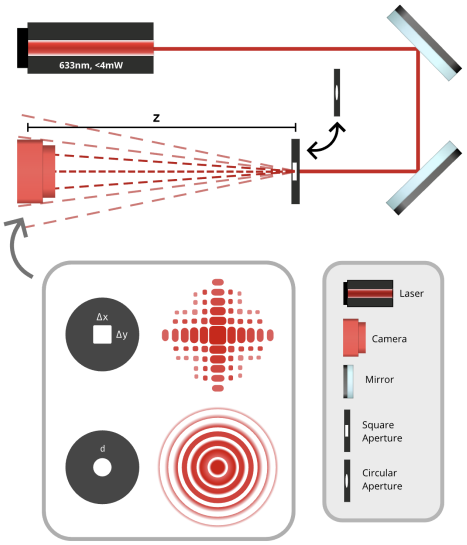

FIG. 4. Experimental setup for diffraction pattern analysis. A 633 nm laser beam is directed through a series of mirrors and apertures before reaching a camera at distance z. The inset shows the resulting diffraction patterns for a square aperture (top) and a circular aperture (bottom), illustrating the characteristic sinc-squared and Airy disk intensity distributions, respectively.

The apertures used were a square aperture with side lengths $\Delta x = \Delta y = 200 \pm 6\,\mu$m, and a circular aperture with a $D = 20 \pm 2\,\mu$m diameter[2, 3]. Each aperture was positioned in the beam path, and its diffraction pattern was recorded at a fixed distance z from the aperture. The diffraction fringes were analyzed using the Fraunhofer approximation.

For accurate wavelength determination, measurements of x, y, and ρ were taken at multiple locations in the diffraction pattern.

To ensure Fraunhofer diffraction conditions, the camera was placed at a sufficiently large distance z based on the aperture dimensions.

Data Collection and Measurement Uncertainty

The diffraction fringe positions (x, y, ρ) were manually selected using a program coded in Processing, a Java-based environment. Processing was chosen over Python for this task due to its built-in image processing functions and ability to more easily create interactive graphical interfaces, which allowed for precise manual selection of diffraction fringes.

I initially attempted to use an automated peak detection method in Python, but it struggled due to secondary maxima and noise affecting the intensity analysis. The algorithm relied on local intensity maxima, which was problematic because exposure levels and background noise led to the algorithm identifying false peaks. Additionally, variations in fringe contrast and spacing across the image led to unreliable peak detection. Moreover, the presence of concentric intensity rings in our captured image (e.g., in Figure 6), possibly from secondary diffraction effects, further complicated automated analysis. Given these challenges, manually selecting the fringe centers and minima using Processing—though inherently limited by human perception—proved to be the more reliable approach, as it allowed for direct visual confirmation and reduced errors introduced by automated intensity-based detection. To improve accuracy, each measurement was taken five times and averaged.

Furthermore, it is crucial to note that in order to obtain the correct results from this analysis, the original images must be used, since the original pixel dimensions may not be preserved, otherwise leading to incorrect estimations of x, y, and ρ in equations (6) and (9).

Part 2: Diffraction from a Reflection and Transmission Grating

To determine the wavelength of the HeNe laser using a diffraction grating, we used both a transmission and a reflection grating. The gratings used in this experiment are listed in Table I.

	Transmission Grating (GT13-03)	Reflective Grating (GH13-24V)
Groove spacing d	3.33 µm	417 nm

TABLE I. Specifications of the transmission and reflective diffraction gratings used in this experiment.

The experimental setup consisted of directing a collimated HeNe laser beam onto the grating surface, measuring the angle θ for the first-order diffracted beam, and applying the grating equation to determine λ. The setup is illustrated in Figure 5, where the diffraction pattern is recorded at a distance z from the grating.

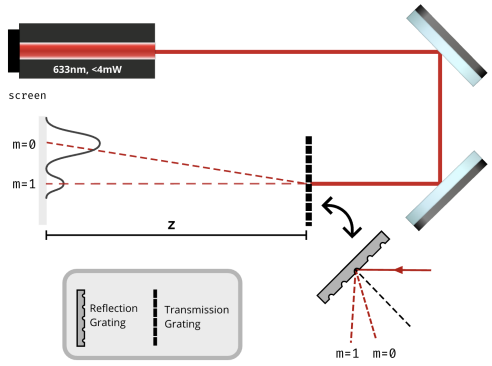

FIG. 5. Experimental setup for diffraction through a transmission and reflection grating, showing relevant fringe orders. The laser beam is directed onto the grating, and the diffraction angles are measured based on fringe positions. The transmission grating produced a non-centered $m = 0$ fringe. A Gaussian intensity profile represents the relative brightness of each order.

RESULTS

Part 1: Diffraction from Square and Circular Apertures

Circular Aperture Diffraction

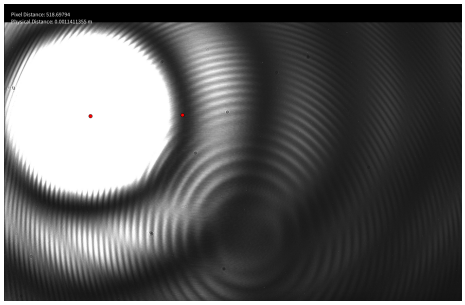

FIG. 6. Sample image showing analysis of diffraction pattern for the circular aperture, with measured fringe separation ρ. The selected points indicate the zeroth-order fringe (central bright spot) and the first minimum used in calculations.

D (µm)	ρ (mm)	z (cm)	λ (nm)
±2	±0.1	±0.3	±104
20	1.141	3.0	623.57
20	1.150	3.0	628.36
20	1.154	3.0	630.67
20	1.141	3.0	623.64

TABLE II. Measured values for the circular aperture diffraction experiment.

Square Aperture Diffraction

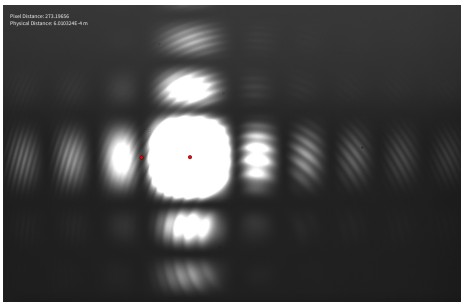

FIG. 7. Sample image showing analysis of diffraction pattern for the square aperture, with measured fringe displacement x in the horizontal direction. Red markers indicate measured points used in wavelength determination.

Δx (µm)	x (mm)	z (cm)	λ (nm)
±6	±0.1	±0.3	±107
200	0.601	19.0	632.67
200	0.592	19.0	623.63

TABLE III. Measured values for the square aperture diffraction experiment in the horizontal direction.

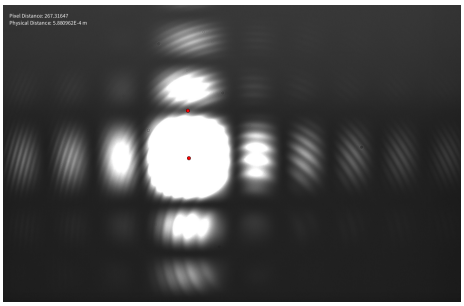

FIG. 8. Sample image showing analysis of diffraction pattern for the square aperture, with measured fringe displacement y in the vertical direction.

Δy (µm)	y (mm)	z (cm)	λ (nm)
±6	±0.1	±0.3	±107
200	0.601	19.0	632.67
200	0.588	19.0	619.05

TABLE IV. Measured values for the square aperture diffraction experiment in the vertical direction.

Part 2: Diffraction from Transmission and Reflection Gratings

Transmission Grating

The transmission grating was placed at a distance $z \approx 42\,\text{cm}$ from the detection screen. The zero-order fringe was taken as the reference point ($m = 0$). The first-order bright fringe ($m = 1$) was displaced by approximately 7.75 cm from the zero-order on the screen. From the geometry in Fig. 2, the diffraction angle was calculated via

$$\theta \;=\; \tan^{-1}\!\Big(\frac{7.75\,\text{cm}}{42\,\text{cm}}\Big) \;\approx\; 10.45^\circ.$$

Since $\lambda = d\,\sin(\theta)$ for $m = 1$, we obtain

$$\lambda \;=\; d\,\sin(10.45^\circ) \;\approx\; 604\,\text{nm}.$$

d (µm)	Δy (cm)	z (cm)	θ (°)	λ (nm)
–	±0.10	±0.10	±0.13	±7
3.33	7.75	42.0	10.45	604

TABLE V. Summary of results for the transmission grating experiment.

Reflection Grating

The reflection grating was placed such that the laser beam was incident at approximately $\theta_{\text{in}} = 45^\circ$. The first-order diffracted beam was found at a distance of 3.3 cm from the zero-order reflection after a propagation of 25.5 cm, yielding

$$\theta_1 \;=\; \tan^{-1}\!\Big(\tfrac{3.3\,\text{cm}}{25.5\,\text{cm}}\Big) \;+\; 45^\circ \;\approx\; 52.37^\circ.$$

Using the reflection-grating equation (12), the wavelength is

$$\lambda \;=\; d\,\big[\sin(45^\circ) + \sin(52.37^\circ)\big] \;\approx\; 625\,\text{nm}.$$

d (nm)	θ_{in} (°)	Δy (cm)	z (cm)	θ_1 (°)	λ (nm)
–	±2.00	±0.10	±0.10	±0.10	±11
417	45.0	3.3	25.5	52.37	625

TABLE VI. Summary of results for the reflection grating experiment.

ANALYSIS

Method	$\overline{\lambda}$ (nm)	σ_λ (nm)	$\lvert\Delta\lambda\rvert$ (nm)	% Error
Square Aperture (Horizontal)	628.15	107	4.85	0.77%
Square Aperture (Vertical)	625.86	107	7.14	1.13%
Circular Aperture	626.56	104	6.44	1.02%

TABLE VII. Comparison of measured HeNe laser wavelengths relative to the known 633 nm for aperture-based methods. $|\Delta\lambda|$ is $|\overline{\lambda} - 633|$, and % Error is $\big(|\Delta\lambda|/633\big) \times 100\%$.

Grating	λ (nm)	σ_λ (nm)	$\lvert\Delta\lambda\rvert$ (nm)	% Error
Transmission	604.0	15	29.0	4.58%
Reflection	625.0	10	8.0	1.26%

TABLE VIII. Comparison of measured HeNe laser wavelengths from the transmission and reflection gratings relative to the known 633 nm. $|\Delta\lambda| = |\overline{\lambda} - 633|$, and % Error $= (|\Delta\lambda|/633) \times 100\%$.

Our measurements confirm that all methods produce results close to the nominal HeNe wavelength of 633 nm but with varying levels of uncertainty and accuracy.

Aperture-Based Methods

The square and circular apertures yielded values in the 619–632 nm range, with typical uncertainties around 100 nm. This relatively large σ_λ stems primarily from the difficulty of identifying the exact first-order minima in smoothly varying diffraction patterns by eye. Small shifts in the chosen fringe center propagate into large changes in λ.

A source of error is that we could not ensure that the laser beam was strictly normal to the apertures. Slight tilt or misalignment often produces additional interference effects—noticeable as concentric fringes in our images. This secondary diffraction superimposes on the primary pattern and complicates the identification of the true first minima. Realigning the laser path to ensure orthogonality to each aperture plane (and verifying it with a beam profiler or alignment telescope) would likely reduce these ring-like artifacts and yield more stable fringe measurements.

Nevertheless, the final averages are all within a few nanometers of 633 nm, providing a simple yet instructive demonstration of diffraction-based wavelength measurement.

Diffraction Gratings

The first-order fringe was easily identifiable, but the measured wavelength ($\approx 604\,\text{nm}$) is notably lower than expected, indicating a $\sim 5\%$ discrepancy. In practice, this is often traced to either an inaccurate z measurement or an alignment error; even a small tilt of the screen or a 1–2 cm mis-measurement in z can shift the calculated θ significantly. An error in z likely arose from difficulty in identifying the camera screen's exact position, which in turn was due to the hooded nature of the camera. This error may have been significant enough to explain the discrepancy in the calculated wavelength.

With the reflection grating, we found $\lambda \approx 625\,\text{nm}$, closer to the expected value, albeit with a higher uncertainty ($\pm 11\,\text{nm}$). Reflection gratings often offer more distinct and higher-contrast diffraction maxima, making angle determination more robust. The clear geometry for incident and diffracted beams likely contributes to the lower percent error. However, we may also have simply made a better estimate of z in this case, leading to a better estimate of λ.

Relative Strengths and Limitations

Despite the large error bars in the aperture methods, they remain straightforward for a quick demonstration and do not require precise knowledge of an angle of incidence. Conversely, while gratings generally yield smaller errors, the result hinges more critically on careful alignment and knowledge of the grating's groove spacing. In this lab, both approaches show that the HeNe laser is near 633 nm, even if the measured standard deviations varied widely.

Potential Improvements

Several refinements could reduce the measurement uncertainties across all setups. One improvement is to implement automated fringe detection, including robust background subtraction and two-dimensional peak-finding, which would help identify the fringe centers with greater accuracy and consistency in the aperture experiments. Another enhancement is to ensure meticulous alignment for every configuration, including the aperture plane and camera plane, in addition to the transmission grating, thereby minimizing systematic offsets in the measured distance z and diffraction angle θ. Finally, repeating measurements with different diffraction gratings and/or additional aperture sizes would expand the parameter space explored, revealing systematic trends or misalignments that might otherwise go undetected and facilitating a more rigorous statistical estimate of both λ and its uncertainty σ_λ. Overall, the reflection grating produced the most consistent accuracy and precision, whereas the transmission grating and apertures were more susceptible to alignment errors. Nevertheless, aperture-based methods remain a straightforward demonstration of diffraction principles, even if their results are more sensitive to subjective fringe selection than the sharply defined maxima of grating-based techniques.

CONCLUSION

All four methods confirmed a wavelength close to 633 nm within a few percent error, validating the applicability of both aperture diffraction and grating-based measurements. The reflection grating stands out for its combination of modest setup complexity and relatively low uncertainty, while the aperture-based approaches illustrate fundamental diffraction physics in a more hands-on but less precise fashion. Future improvements could focus on stricter alignment procedures and more advanced image analysis to reduce uncertainties and systematic offsets.

BIBLIOGRAPHY

[1] Thorlabs, Inc., "Helium Neon Lasers," Accessed March 1, 2025. https://www.thorlabs.com/newgrouppage9.cfm?objectgroup_id=10776

[2] Thorlabs, Inc. "Precision Square Apertures." Accessed March 15, 2025. https://www.thorlabs.com/newgrouppage9.cfm?objectgroup_id=14494

[3] Thorlabs, Inc. "Precision Circular Apertures." Accessed March 15, 2025. https://www.thorlabs.com/newgrouppage9.cfm?objectgroup_id=14350

[4] Edmund Optics. "Allied Vision Alvium 1800 U-500M Camera Specifications." Accessed March 15, 2025. https://www.edmundoptics.ca/p/allied-vision-alvium-1800-u-500m-125-50mp-c-mount-\protect\penalty\z@right-angle-usb-31-monochrome-camera/42327

Acknowledgements

These experiments were performed in collaboration with Aleksandar Radak, Cameron Brown, and Bhavya Chugh.